Upgrade of the relative calibration methods and Bayesian inference processing for electron cyclotron emission radiometry

Xin Yu[1], *Zhongbing Shi*[1*], *Zengchen Yang*[1], *Min Jiang*[1], *Wei Chen*[1], *Tianbo Wang*[1], and *Wenan Pan*[1]

[1]Southwestern Institute of Physics, Chengdu 610041, China

Abstract. An upgraded local oscillator (LO) hopping calibration method based on a blackbody hot source and a perturbation analysis of the magnetic field difference method are introduced in this work. The blackbody hot source is used to evaluate the difference in the relative coefficients between the two LO hopping frequencies in the same channels. Then the coefficients are obtained by multiplying the LO hopping frequencies coefficients by LO hopping calibration coefficients. In this way, it is more flexible and stable than the in-situ calibration using the blackbody hot source. The magnetic field difference method is also convenient as another calibration method to obtain the relative calibration coefficients of the electron cyclotron emission radiometers (ECE). In general, the magnetic field difference method needs two similar shots but a difference of 2.1% (for HL-2M) in the magnetic field. Meanwhile, there are some errors because of the inconsistent detection positions in the same channels between the two shots. For evaluating the calibration errors, the impact of the displacement, T_e perturbation of the core region, and magnetic field difference has been discussed. The result shows that a larger magnetic field difference can improve the accuracy of the calibration. In the end, Bayesian inference has been utilized to evaluate the calibration coefficients and get the most probable calibration coefficients and the confidence interval.

1 Introduction

ECE radiometry is a powerful T_e and T_e perturbation (δT_e) diagnostic with high spatial-temporal resolution and it has been established on many tokamaks [1-4]. The calibration of the ECE radiometry is the key step in obtaining the absolute or relative T_e profile. The conventional calibration method is the in-situ calibration using the blackbody hot source with known temperature and it is utilized on many devices such as JET, DIII-D, EAST, and ITER (in the future) [5-8]. However, the blackbody hot source method is complex and inflexible because it requires a long time operation (tens of minutes or even hours) and enough space to operate. Therefore, handy and flexible relative calibration methods like the LO hopping and magnetic field difference method are meaningful [9].

Following the introduction section, an upgraded LO hopping calibration method will be described in Section 2. The perturbation analysis for the magnetic field difference method will be discussed in Section 3. In Section 4, Bayesian inference for the relative calibration methods will be introduced. Finally, Section 5 presents the summary.

2 Upgraded LO hopping method

The principle of the LO hopping method is comparing the signal amplitude between the adjacent channels in the same measurement position by hopping the LO frequency. However, the mixer efficiency varies with the LO frequency which also results in different initial bias voltages at different LO frequencies. In the strict sense, there are many elements varying with the different LO frequencies such as the antenna gain, transmission loss, and electronic response (including the mixer's efficiency). Therefore, merely comparing the signal amplitude is not complete which will cause prominent calibration errors. The upgraded LO hopping calibration method uses a blackbody hot source to evaluate the response of the measurement channels to different LO frequencies. With this method, the relative T_e can be derived as below:

$$I_i(f_i) \times C_i(f_i) = T_e(f_i) \quad (1)$$

$$I_i(f_{i+1}) \times C_i(f_{i+1}) = T_e(f_{i+1}) \quad (2)$$

$$I_{i+1}(f_{i+1}) \times C_{i+1}(f_{i+1}) = T_e(f_{i+1}) \quad (3)$$

$$I_{bi}(f_i) \times C_i(f_i) = T_b(f_i) \quad (4)$$

$$I_{bi}(f_{i+1}) \times C_i(f_{i+1}) = T_b(f_{i+1}) \quad (5)$$

Then we get :

$$S_i = \frac{C_i(f_{i+1})}{C_i(f_i)} = \frac{T_b(f_{i+1}) \times I_{bi}(f_i)}{I_{bi}(f_{i+1}) \times T_b(f_i)} \quad (6)$$

$$C_{i+1}(f_{i+1}) = \frac{I_i(f_{i+1}) \times C_i(f_{i+1})}{I_{i+1}(f_{i+1})} = \frac{I_i(f_{i+1}) \times S_i \times C_i(f_i)}{I_{i+1}(f_{i+1})} \quad (7)$$

Where I, C, f, I_b, T_b, S, and i are the plasma ECE signal amplitude, calibration coefficients, radiation frequency, radiation amplitude of the blackbody hot source, radiation temperature of the blackbody hot source, LO hopping calibration coefficients ratio, and the channel number, respectively. Setting the C_1 to 1, the relative calibration coefficients can be derived with Eq. 7.

Normally, the blackbody hot source's in-situ absolute calibration is the conventional calibration method for ECE radiometry. However, the absolute calibration coefficients change slowly over time because of the change in the response of the radiation frequency (RF) amplifier, intermediate frequency (IF) amplifier (mainly caused by active devices), the loss of the transmission line, window coating, and so on. It can be approximatively described as follow:

$$C_i(t,f_i) = C_i(0,f_i) \times RFA_i(t,f_i) \times RFM_i(t,f_i) \times IFA_i(t,f_i) \times IFM_i(t,f_i) \times L_i(t,f_i). \quad (8)$$

In the above, the $C_i(0)$ is the initial coefficient. The t, RFA, RFM, IFA, IFM, and L are the time, the relative variation coefficients of the RF amplifier, RF mixer, IF amplifier, IF mixer, and the loss of the transmission, respectively. Generally, the variation of the response of those active microwave devices is independent so that the response of the whole working band enhances or abates independently. For a frequency interval of 1 GHz (the interval of IF), the response variable of the active microwave devices and transmission loss can be approximatively considered to be linear. Therefore, Eq. 8 can be simplified as:

$$C_i(t,f_i) = C_i(0,f_i) \times RFA(t) \times RFM(t) \times IFA_i(t) \times IFM_i(t) \times L(t). \quad (9)$$

The relative variation ratio of the calibration coefficients in the two hopping LO frequencies (S_i) can be derived as below:

$$S_i = \frac{C_i(t,f_{i+1})}{C_i(t,f_i)} = \frac{C_i(0,f_{i+1})}{C_i(0,f_i)}. \quad (10)$$

This means the S_i does not vary with time or vary very slowly. It should be noted that IFA_i and IFM_i can vary differently in different channels which induces a difference in the relative coefficients between different channels:

$$\frac{\frac{C_i(t,f_i)}{C_i(0,f_i)}}{\frac{C_j(t,f_j)}{C_j(0,f_j)}} = \frac{IFA_i(t) \times IFM_i(t)}{IFA_j(t) \times IFM_j(t)} \neq constant. \quad (11)$$

Where the j represents another channel. Therefore, the blackbody hot source's in-situ absolute calibration needs to be conducted once in a while, but the upgraded LO hopping relative calibration uses the blackbody hot source just once.

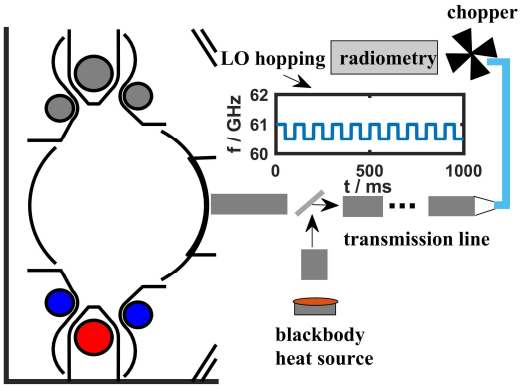

Fig. 1. Schematic diagram of obtaining the relative variation ratio of the calibration coefficients in the two hopping LO frequencies.

As shown in Fig. 1, a mirror is utilized to transmit the radiation generated by the blackbody hot source to the radiometry from the transmission line. The radiation signal is hopping by the chopper. Subsequently, comparing the signal intensity in different LO hopping frequencies, the S_i can be obtained by Eq. 6. The schematic diagram of the upgraded LO hopping calibration is shown in Fig. 2. The measurement positions are constant between two adjacent channels in the two LO hopping frequencies (LO_1, LO_2). Therefore, the relative calibration coefficients can be derived by Eq. 7 and the S_i can be used to calibrate several times without blackbody hot source evaluation.

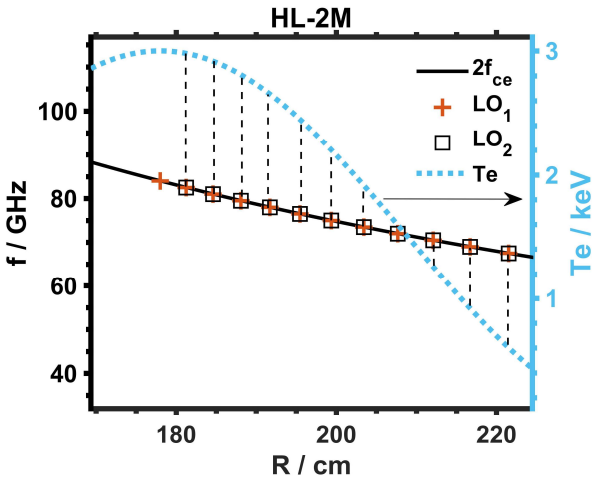

Fig. 2. Schematic diagram of the upgrade LO hopping relative calibration.

3 Perturbation analysis of the magnetic field difference method on HL-2M

The magnetic field difference method is another relative calibration method for the ECE which is very handy and flexible. Generally, the calibration coefficients are obtained by comparing the signal intensity in the same discharge parameters with an appropriate magnetic field difference. Normally, the appropriate magnetic field difference is dependent on the minimum of the mean of the position deviation (δR_m) between the adjacent channels with the change of the magnetic field in two shots as shown in Fig. 3. The B_{t00} and B_{t01} are the

calibration magnetic fields on the magnetic axis. The relative calibration coefficients can be obtained below:

$$C_{i+1} = C_i\left(\frac{\frac{2I_{Ai}}{R_{Ai}-R_{Bi+1}} - \frac{I_{Ai}-I_{Bi}}{R_{Ai}-R_{Bi}}}{\frac{2I_{Bi+1}}{R_{Ai}-R_{Bi+1}} + \frac{I_{Ai+1}-I_{Bi+1}}{R_{Ai+1}-R_{Bi+1}}}\right) \quad (12)$$

In the above, the I_A, I_B, and R_A, R_B are the ECE signal intensities and the measurement positions in the two shots, respectively. Unfortunately, the position deviation always exists since the variation of the magnetic field causes different changes in the detected location for the different radial channels. Consequently, the calibration coefficients obtained by this method are not very accurate. Theoretically, sweeping the magnetic field rapidly, the radiometry can measure the same positions in adjacent channels. In fact, it is difficult for the toroidal magnetic coils, especially for superconducting toroidal magnetic coils.

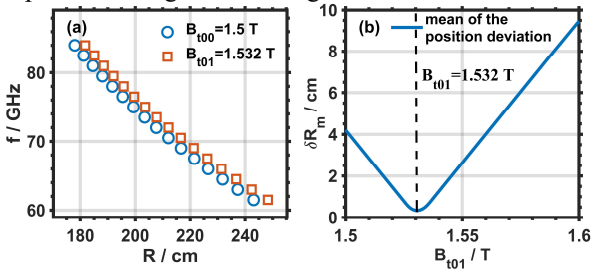

Fig. 3. Calibration of multi-channel ECE radiometry by magnetic field difference method. (a) Measured positions at B_{t00} = 1.5 T and B_{t01} = 1.532 T, (b) The position deviation between adjacent channels (δR_m) as B_{t01} increases from 1.5 T to 1.6 T.

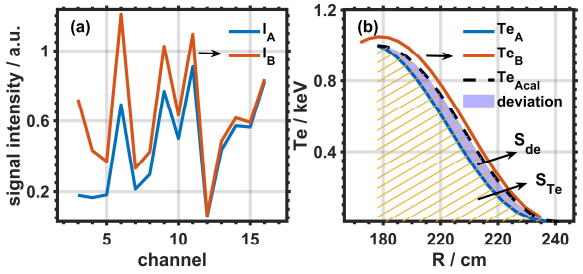

Fig. 4. Schematic diagram of the perturbation analysis of the magnetic field difference method. (a) The signal intensity of different channels. (b) Calibration results with the magnetic field difference method.

However, the perturbation analysis shows that the magnetic field difference in which the δR_m reaches up to the minimum is not the most appropriate. FIGURE. 4. (a) shows the signal intensities obtained from the preset T_e profiles (T_{eA}, T_{eB}) in Fig. 4. (b). The I_A is set as a random series and the I_B is obtained by

$$I_B = \frac{T_{eB} \times I_A}{T_{eA}} \quad (13)$$

About the preset profiles, they are fitted using the standard temperature profile:

$$T_e = T_e(0)\left(1 - \left(\frac{r}{a}\right)^2\right)^{\alpha} \quad (14)$$

Where r is the minor radius, a = 65 cm, and α is set up to 2.7. The core T_e (T_{e0}) and the magnetic axis positions (R_0) are set as 1 keV, 178 cm for the T_{eA}, and 1.05 keV, 179 cm for the T_{eB}, presumably induced by the plasma displacement or other physical problems. The dashed line shown in Fig. 4. (b) is the calibrated T_e (T_{eAcal}) profile regarding the T_{eA}. The shadowed area is the deviation between the T_{eA} and the T_{eAcal}. Therefore, the error is defined as the ratio of the deviation area to the T_e profile area (S_{de}/S_{Te} as shown in Fig. 4. (b)) and the accuracy is defined as 1- S_{de}/S_{Te}. By setting up the T_{e0A} = 1 keV, R_{0A} = 178 cm, and B_{t0A} = 1.5 T, scanning the R_{0B}, T_{e0B}, and B_{t0B} from 173 cm to 183 cm, 0.8 keV to 1.2 keV and 1.2 T to 1.8 T, the calibration accuracy depending on the R_{0B}, T_{e0B}, and B_{t0B} can be obtained as shown in Fig. 5. (the T_{e0A}, T_{e0B}, R_{0A}, R_{0B}, B_{t0A}, and B_{t0B} are the T_{e0}, R_0, and B_{t0} of the T_{eA} and T_{eB}).

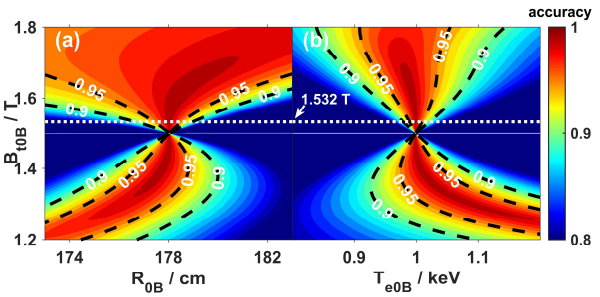

Fig. 5. The dependence of calibration accuracy on (a) R_{0B} and B_{t0B} (T_{e0B} = T_{e0A}), (b) T_{e0B} and B_{t0B} (R_{0B} = R_{0A}) where T_{e0A} = 1 keV, R_{0A} = 178 cm, and B_{t0A} = 1.5 T.

FIGURE 5(a) and (b) show the dependence of calibration accuracy on the R_{0B}, T_{e0B}, and B_{t0B}. The thick dashed lines display the contour lines of the calibration accuracy of values 0.95 and 0.9, and the dotted line displays the contour of the B_{t0B} = 1.532 T which the mean of the deviation reaches the minimum. The calibration accuracy is more dependent on the T_{e0B} and it is difficult for the calibration accuracy to reach 0.95 when the B_{t0B} = 1.532 T for both the R_{0B} and B_{t0B}. Higher B_{t0B} can expand the range of accurate calibration.

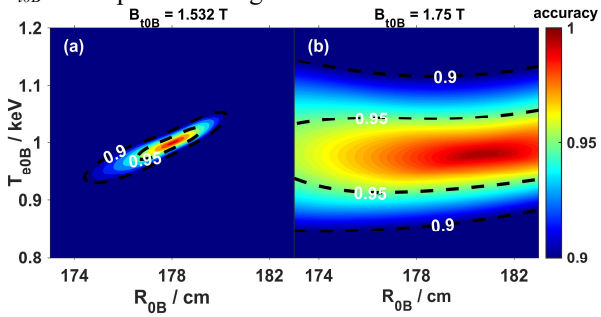

Fig. 6. The dependence of calibration accuracy on R_{0B} and T_{e0B} when (a) B_{t0B} = 1.532 T and (b) B_{t0B} = 1.75 T, where T_{e0A} = 1 keV, R_{0A} = 178 cm, and B_{t0A} = 1.5 T.

FIGURE 6(a) and (b) show the dependence of the calibration accuracy on the R_{0B} and T_{e0B} when B_{t0B} equals 1.532 T and 1.75T. Apparently, 1.532 T is not the most appropriate B_{t0B} for this calibration method because the allowable range is much more narrow than the case of B_{t0B} = 1.75 T compared to Fig. 6. (b).

FIGURE 6(b) shows that for the calibration accuracy of 0.95, the R_{0B} and T_{e0B} can vary in the range of 173 - 183 cm and 0.95 - 1.05 keV approximately. In other

words, the position deviation and variation of the T_{e0} between the two calibration shots caused by the plasma displacement or the difference of the discharges are allowed to deviate by 5 cm on R_0 and 5% on T_{e0} for 95% calibration accuracy, which is acceptable for the control on the tokamak plasma.

The perturbation analysis shows the possibility of accurate calibration of the T_e profile using this method. It's worth noting that, the accurate calibration range with this method depends on many elements, for example, the geometric dimensioning of the plasma, the working magnetic field, and the working frequency band of the ECE radiometry. Therefore, the perturbation analysis needs to be performed before the calibration to get an appropriate magnetic field difference. Due to the convenience and flexibility, the magnetic field difference method is chosen as one of the calibration methods for ECE radiometry on HL-2M to access the calibration coefficients.

4 Bayesian inference processing

In order to evaluate the calibration coefficients obtained by the upgraded LO hopping method or magnetic field difference method, the Bayesian inference [10] is utilized to process the calibration data. Normally, the calibration coefficient C_{im} depends on the measured temperature T_{ei}, signal intensity I_{im}, and the systematic and statistical errors ε_i (the i and m denote the channel number and calibration number):

$$C_{im} = {}^{T_{ei}}/_{I_{im}} + \varepsilon_i \tag{15}$$

As mentioned above, it can be solved by the Bayesian theory:

$$p(T_e \mid C, \theta) \propto p(C \mid T_e, \theta) \cdot p(T_e \mid \theta) \tag{16}$$

In the above, the θ, $p(T_e \mid C, \theta)$, $p(C \mid T_e, \theta)$, and $p(T_e \mid \theta)$ are the additional information for inferences, posterior probability distribution, likelihood probability distribution, and prior probability distribution. In the Gaussian Process method, the $p(C \mid T_e, \theta)$ and $p(T_e \mid \theta)$ can be formulated by Gaussian Processes (GP):

$$p(C \mid T_e, \theta) = \frac{1}{|\Sigma_c|^{\frac{1}{2}}(2\pi)^{\frac{n}{2}}} \exp\left[-\frac{\left({}^{T_e}/_{I}-C\right)^T \Sigma_C^{-1}\left({}^{T_e}/_{I}-C\right)}{2}\right] \tag{17}$$

$$p(T_e \mid \theta) = \frac{1}{|\Sigma_{Te}|^{\frac{1}{2}}(2\pi)^{\frac{n}{2}}} \exp\left[-\frac{(T_e-\mu_{T_e})^T \Sigma_{Te}^{-1}(T_e-\mu_{T_e})}{2}\right] \tag{18}$$

In the above equation, the n and μ_{Te} are the number of the channels and expected temperature, respectively. The Σ_c and Σ_{Te} are the calibration uncertainty and inference uncertainty covariance matrixes, respectively. They are denoted as:

$$\Sigma_c = \begin{bmatrix} C_{e1}^2 & \cdots & 0 \\ \vdots & \ddots & \vdots \\ 0 & \cdots & C_{en}^2 \end{bmatrix}, \tag{19}$$

$$\Sigma_{T_e} = \begin{bmatrix} kf(1,1) & \ldots & kf(1,n) \\ \vdots & \ddots & \vdots \\ kf(n,1) & \ldots & kf(n,n) \end{bmatrix}, \tag{20}$$

$$kf(i,j) = \sigma_{T_e}^2 \exp\left(-\frac{d_{ij}^2}{2\sigma_l^2}\right), d_{ij} = |R_i - R_j| \tag{21}$$

In the above, the C_{ei}, and R_i, R_j are the calibration errors and the measured positions, respectively. The $\sigma_{T_e}^2$ and σ_l^2 are the hyperparameters obtained by Occam's razor optimization criterion. Consequently, the combination of the prior and likelihood is derived as below:

$$p(T_e \mid C, \theta) \propto p(C \mid T_e, \theta) \cdot p(T_e \mid \theta) \propto \exp\left[-\frac{\left({}^{T_e}/_{I}-C\right)^T \Sigma_C^{-1}\left({}^{T_e}/_{I}-C\right)}{2}\right] \exp\left[-\frac{(T_e-\mu_{T_e})^T \Sigma_{Te}^{-1}(T_e-\mu_{T_e})}{2}\right] \tag{22}$$

The expected number $(\mu_{T_e}^*)$ and covariance matrix $(\Sigma_{T_e}^*)$ of the prior can be derived as:

$$\begin{cases} \mu_{T_e}^* = \mu_{T_e} + \left({}^{1}/_{I}{}^T \cdot \Sigma_C^{-1} \cdot {}^{1}/_{I} + \Sigma_{Te}^{-1}\right)^{-1} {}^{1}/_{I}{}^T \cdot \Sigma_C^{-1} \\ \qquad \cdot \left(C - {}^{1}/_{I} \cdot \mu_{T_e}\right) \\ \Sigma_{T_e}^* = \left({}^{1}/_{I}{}^T \cdot \Sigma_C^{-1} \cdot {}^{1}/_{I} + \Sigma_{Te}^{-1}\right)^{-1} \end{cases} \tag{23}$$

Experimentally, a magnetic field difference relative calibration is processed with Bayesian inference on HL-2A. The data points are the 100 times calibration in a stable discharge period of 200 ms. FIGURE 7 shows the processing result. The shadowed area is the 95% confidence interval and the solid line is the expected value of the highest probability. It can be seen that the maximum probability profile is different from the mean of the original samples and it is more smooth. The maximum uncertainty comes from the core region of the plasma. Bayesian inference provides a method with a confidence interval to determine the calibration coefficients and is helpful to evaluate the calibration accuracy.

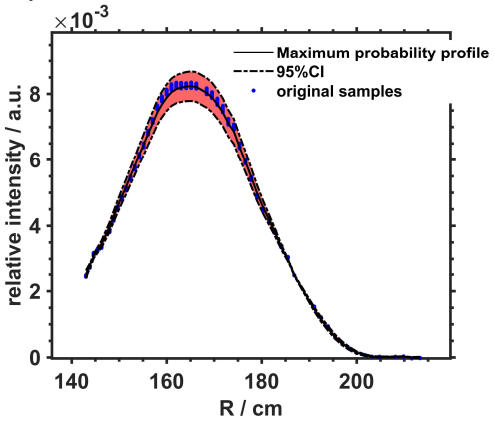

Fig. 7. Bayesian inference result of the magnetic field difference method on HL-2A. (the solid line is the relative T_e of maximum probability, and the area between the dash lines is a 95% confidence interval.)

5 Summary

An upgraded LO hopping calibration method utilizes the blackbody hot source to evaluate the relative variation ratio of the calibration coefficients in the two hopping LO frequencies. The absolute coefficients can be obtained by simple ratio calculation. The advantage of this method is more flexible and stable. The perturbation analysis of the magnetic field difference method shows that the magnetic field when the mean of the position deviation reaches the minimum is not the most appropriate. By perturbation analysis, the most appropriate magnetic field and the allowable range of errors are obtained. In the case of this analysis, the position deviation and variation of the T_{e0} between the two calibration shots caused by the plasma displacement or the difference of the discharges are allowed to deviate by 5 cm on R_0 and 5% on T_{e0} for 95% calibration accuracy. It is acceptable for the control of the tokamak plasma. In addition, the Bayesian inference processing has been simply utilized to evaluate the calibration coefficients. The result shows that the maximum probability profile is different from the mean of the original samples and it is more smooth. The maximum uncertainty comes from the core region of the plasma. Therefore, it can provide a method with a confidence interval to determine the calibration coefficients and helps us to evaluate the calibration accuracy. The experimental verification will be carried out at the end of 2022.

6 Acknowledgments

This work is supported by the National Magnetic Confinement Fusion Science Program of China (Grant Nos. 2017YFE0301203), the National MCF Energy R&D Program (No. 2022YFE03060000), the Sichuan Science and Technology Program (Nos. 2021JDJQ0029), and the National Natural Science Foundation of China (Grant Nos. 12175055 and Grant Nos. 12075079).

References

1. Z. B. Shi, W. L. Zhong, M. Jiang, Plasma Sci. Technol. **20**, 094007 (2018)
2. Z. J. Yang, X. M. Pan, X. D. Ma, B. W. Ruan, R. B. Zhou, and C. Zhang, Rev. Sci. Instrum. **87**, 11E112 (2016)
3. S. J. Freethy, G. D. Conway, I. Classen, A. J. Creely, T. Happel, A. Köhn, B. Vanovac, and A. E. White, Rev. Sci. Instrum. **87**, 11E102 (2016)
4. D. D. Truong, and M. E. Austin, Rev. Sci. Instrum. **85**, 11D814 (2014)
5. S. Schmuck, J. Fessey, T, Gerbaud, et al, Rev. Sci. Instrum. **83**, 125101 (2012)
6. M. E. Austin, R. F. Ellis, J. L. Doane, et al, Rev. Sci. Instrum. **68**, 480 (1997)
7. Y. Liu, S. Schmuck, H. Zhao, et al, Plasma Sci. Technol. **18**, 1148 (2016)
8. G. Taylor, M. E. Austin, A. Basile, et al, EPJ Web of Conferences. EDP Sciences, **147**, 02003 (2017)
9. Z. B. Shi, et al. Rev. Sci. Instrum. **85**, 023510 (2014)
10. M. A. Chilenski, M. Greenwald, Y. Marzouk, et al, Nucl. Fusion, **55**, 023012 (2015)